Pergamon

0038-1101(95)00238-3

Solid-State Electronics Vol. 40, Nos 1–8, pp. 161–165, 1996

0038-1101/96 $15.00 + 0.00

DYNAMICS OF ELECTRIC-FIELD DOMAINS AND CHAOS IN SEMICONDUCTOR SUPERLATTICES

L. L. BONILLA, O. M. BULASHENKO, J. GALÁN, M. KINDELAN and M. MOSCOSO
Escuela Politécnica Superior, Universidad Carlos III de Madrid, Butarque 15, 28911 Leganés, Spain

Abstract—A discrete drift model of sequential resonant tunneling in weakly-coupled doped or undoped GaAs/AlAs superlattices (SL) under d.c. or d.c. + a.c. voltage bias and laser illumination is analyzed. In agreement with experiments our model shows an oscillatory I–V diagram for large enough values of the doping and/or laser illumination, multistability and hysteresis between stationary solutions and self-sustained time dependent oscillations of the current. Numerical and asymptotic analyses of the model show that these current oscillations are due to the formation, motion, annihilation and regeneration of negatively charged domain walls on the SL. For appropriate d.c. + a.c. voltage bias, chaotic current oscillations with loss of spatial coherence of the electric field will appear due to random nucleation of domains in the SL.

The formation of stable electric-field domains in doped and undoped semiconductor superlattices has been intensively investigated both experimentally[1–4] and theoretically[5–8]. Unstable domain distributions in superlattices, however, have only been discovered very recently. Damped current oscillations are present in undoped superlattices under large photoexcitation [4], and, for certain values of the doping, self-oscillations of the current appear[9].

In this work we present additional results for a recently proposed discrete drift model[6] that accounts in a satisfactory way for the stationary and dynamical properties of semiconductor superlattices, paying special attention to the connection with the available experimental results. We also stress the convenience of studying the continuum limit of the model in order to gain some insight on the dynamical behavior of the system (preliminary results for the continuum limit including an equal-area-rule for the velocity of domain walls were announced in Ref. [8]). Finally, we find that when the system is additionally driven by an a.c. field, new interesting dynamical phenomena appear, namely, chaotic motion of electric field domains due to random nucleation of charge monopole waves over the whole structure[10]. The maximum number of monopoles that can be simultaneously present in a chaotic situation varies from two to three with the number of wells of the SL. This seems to be related with the loss of spatial coherence and the fractal dimension of the attractor. For long enough SLs, the fractal dimensions of the chaotic attractors do not change appreciably with the SL length, which implies that the predicted chaos depends on few effective degrees of freedom.

We consider a set of weakly interacting quantum wells characterized by values of the electric field E_j the electron densities n_j and the hole densities p_j with $j = 1, \ldots, N$ denoting the well index.

This mean-field-like approach is justified because for the high voltages involved the tunneling process is sequential and the electron loses coherence before leaving the well. Besides, the relevant time scale for the oscillations ($\sim 0.1\ \mu$s) and the dynamics of the electric field domains in a weakly coupled SL are much larger than those for the tunneling process between adjacent wells (~ 1 ns) and the relaxation from excited levels to the ground state within each well (~ 1 ps). Therefore, a single quantum well reaches a situation of local equilibrium between two consecutive tunneling processes.

The one-dimensional equations governing the dynamics of the system are the Poisson equation averaged over one SL period, Ampère's equation for the balance of current density J (hole current is neglected), a rate equation for the holes, and the voltage bias condition

$$E_j - E_{j-1} = \frac{el}{\epsilon}(n_j - p_j - N_D), \tag{1}$$

$$\epsilon \frac{dE_j}{dt} + ev(E_j)n_j = J, \tag{2}$$

$$\frac{dp_j}{dt} = \gamma - rn_j p_j, \tag{3}$$

$$l\sum_{j=1}^{N} E_j = V, \tag{4}$$

where e, l, r and ϵ are the electron charge, superlattice period, electron–hole recombination rate and effective dielectric constant, respectively. N_D, γ and V are external parameters that represent the doping, photogeneration rate and external voltage. The effective electron velocity $v(E)$ (proportional to the tunneling probability) exhibits maxima at the resonant fields for which the adjacent levels of neighboring wells are aligned[6]. Those resonances are purely quantum

mechanical phenomena that have to be included necessarily in our otherwise semiclassical model. Notice the importance of the negative differential conductance (NDC) region in the velocity curve giving rise to current instabilities in the SL.

The boundary condition at the first contact, $\epsilon(E_1 - E_0)/(el) = n_1 - p_1 - N_D = \delta$, allows for a small negative charge accumulation in the first wall ($\delta \ll N_D$). The physical origin of δ is clear for an n^+-n-n^+ structure: due to the different electron concentrations at each side of the first barrier, some charge will be transferred from the contact to the first quantum well. This creates a small dipole field, which cancels the electron flow. For a p-i-n structure a flat boundary condition ($\delta = 0$) which avoids charge accumulation should be used[4].

The model eqns (1)–(4) have been solved numerically and the results will be presented below in dimensionless form by adopting as the unit of field the value $E_{1-2} = \Delta\epsilon_{12}/(el)$, with $\Delta\epsilon_{12}$ being the energy separation between the first and the second electron subbands [the maximum of $v(E)$]. This yields the characteristic charge density $n_0 = \epsilon E_{1-2}/(el)$ used to normalize the carrier and the doping concentrations. Finally for J, γ and V the units are $en_0 v(E_{1-2})$, rn_0^2 and $E_{1-2}Nl$, respectively.

The two most common experimental probes used to investigate the behavior of the SL are current and photoluminescence measurements. The first one can be time resolved (in the 0.1 ns regime), time averaged, with photogenerated carriers or with electronic doping of the sample. All of these possibilities can be described within our model. The second one (time resolved or averaged) gives an integrated information about the electric field on the wells over the whole sample, by means of the Quantum Confined Stark Effect[3].

In Fig. 1 we plot the calculated current vs the applied d.c. voltage for three different laser powers ($\gamma = 0$; 1×10^{-2} and 4×10^{-2}), obtained using the velocity vs field curve shown in the inset, and which is related to the experimental current–voltage characteristic[9]. Since we are interested in depicting the self-sustained current oscillations under the fields above E_{1-2}, we have ignored the small maximum of $v(E)$ near $E = 0$ correspondent to miniband conduction. The calculated current without photoexcitation exhibits oscillations as observed in the experiment. The time integrated I–V characteristic has been obtained by averaging the value of the current over one period of the oscillation. As in the experiments, the fine structure of the I–V curve appears when additional carriers are introduced by photoexcitation, that means the oscillations die out under higher concentration of carriers.

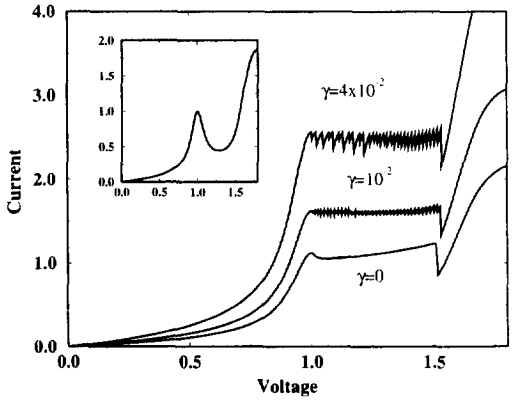

Fig. 1. Calculated I–V characteristic for three different photoexcitation intensities as indicated and doping $v = 0.1$. Inset: dimensionless $v(E)$ curve used in the simulation. This curve coincides with the I–V characteristic for $v < 0.04$.

Let us now consider the results for doped SL without photoexcitation. For this case we found undamped current oscillations for appropriate values of the bias only for the doping density v between 0.04 and 0.15. Below 0.04 the SL evolves from any initial condition to a uniform state with the same constant values of charge and field in each well. Above $v = 0.15$ stable electric field domains are formed. This limit can also be described by means of a discrete mapping as in Ref. [6]. For in-between values, we find undamped oscillations of frequency ≈ 10 MHz in close agreement with the experimental results for an $N = 40$-well 9 nm GaAs/4 nm AlAs SL[9]. Within the NDC region the only stable solution corresponds to the undamped current oscillations. However, outside the NDC region, we find a narrow region of bistability and hysteresis between the undamped current oscillations and a stationary solution.

In Fig. 2(a–e) we plot the calculated electric field profiles at different times of one period of the current

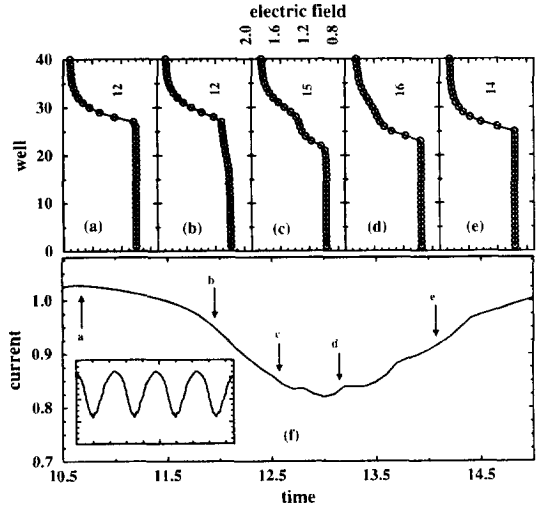

Fig. 2. Electric field profiles and absolute value of the current during one time-period of the oscillation (calculated frequency: 10 MHz). (a)–(e) Electric field profiles at the times marked with arrows in (f). The digits under the curves indicate the number of wells in the high field region ($E > 1.3$). Insets in (f): current oscillations showing several complete periods.

oscillation, which is depicted in Fig. 2f, for a dimensionless doping density of $v = 0.1$ (corresponding to the average over the SL $N_D \approx 1.15 \times 10^{17}\,\mathrm{cm}^{-3}$) and no laser illumination. One can see that a larger current corresponds to a larger extension of the low-field domain, whereas low current indicates a larger extension of the high-field domain. This agrees very well with the experimental results for a $N = 40$ well 9 nm GaAs/4 nm AlAs SL[9].

The self-sustained oscillations are due to a recycling (deep inside the SL) and motion (toward the end of the SL) of the domain wall (charge monopole) separating low and high-field regions. The recycling is more clearly seen in Fig. 3a, where the time evolution of the electron density is represented: the peaks of the electron density show where the centers of the domain walls are. During each period a domain wall is formed inside the SL. It then moves forward towards the corresponding contact. Depending on the applied voltage, it may or may not reach the end of the SL before it disappears and another monopole is formed starting a new period of the oscillation. Simulations clearly show monopole recycling with two monopoles coexisting during some part of one current oscillation period (see Fig. 3a). The frequency of the oscillation is mainly determined by the number of quantum wells the monopole moves across and by the average drift velocity[8]. The amplitude of the current oscillation is proportional to the difference between the maximum and minimum of the velocity curve.

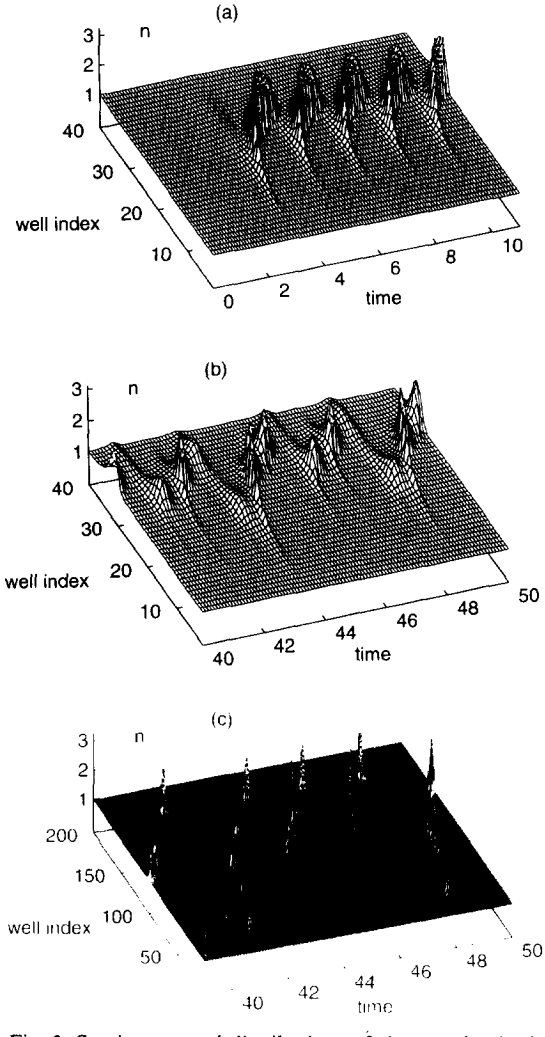

Fig. 3. Spatio-temporal distributions of electron density in a doped SL without photoexcitation for: (a) pure d.c. bias on a $N = 40$ SL, (b) d.c. + a.c. bias with $a = 0.09$ and $N = 40$, (c) d.c. + a.c. bias with $a = 0.12$ and $N = 200$.

Monopole recycling can be studied asymptotically and numerically for long SLs[8]. Instead of an apparent deformation of the domain wall as in Fig. 2 (c, d), a spatially-extended flat region with intermediate field appears between the low and high-field domains during part of each oscillation period. In addition, the small charge accumulation at the first well plays an essential role in the development of the current oscillations. The field behind the monopole is uniform in space, up to a small correction of the order of δ near the boundary. When the current reaches its maximum, the field behind the monopole takes the values on the NDC region, and those corrections increase exponentially in time, giving to a new monopole. For very long SLs an asymptotic calculation shows that the monopoles are formed and destroyed in time scales much shorter than their travelling time towards the end of the SL. Ignoring these fast stages of the oscillation, the values of the electric field on the domains separated by a domain wall are approximately given by the zeros of $ev(E)N_D - J$. As there are three such zeros $J/(eN_D)$ between the maximum and minimum of the velocity curve, then we may have coexistence of, at most, two monopoles separating three electric field domains.

Having found a system with a natural oscillation due to traveling-wave motion, it is natural to ask whether harmonic forcing would lead to chaos with spatial structure. The answer is affirmative. We start with a uniform initial field profile and solve the equations for d.c. bias. After a short transition, the self-sustained oscillations set in and we switch on the additional a.c. microwave signal of relative amplitude a and frequency f_d, so the net a.c. + d.c. voltage will be $V\{1 + a\sin(2\pi f_d t)\}$.

Our main result is that the competition between the natural oscillation due to monopole dynamics and the forcing gives rise to narrow windows of spatio-temporal chaos for appropriate values of V, a and f_d (see also Ref. [10]). Let us fix the ratio between the natural frequency f_0 and the driving frequency f_d at the golden mean $(\sqrt{5}-1)/2$, and the voltage V at 1.2. The loss of spatial coherence in the chaotic regime can be seen in Fig. 3b, where the electron concentration as a function of time and well index is presented for the case of d.c. + a.c. driving (time is in units of the period of the a.c. driving, $T_d = 1/f_d$). For $N = 40$ wells at most two monopoles are simultaneously present on the SL: the maximum distance between

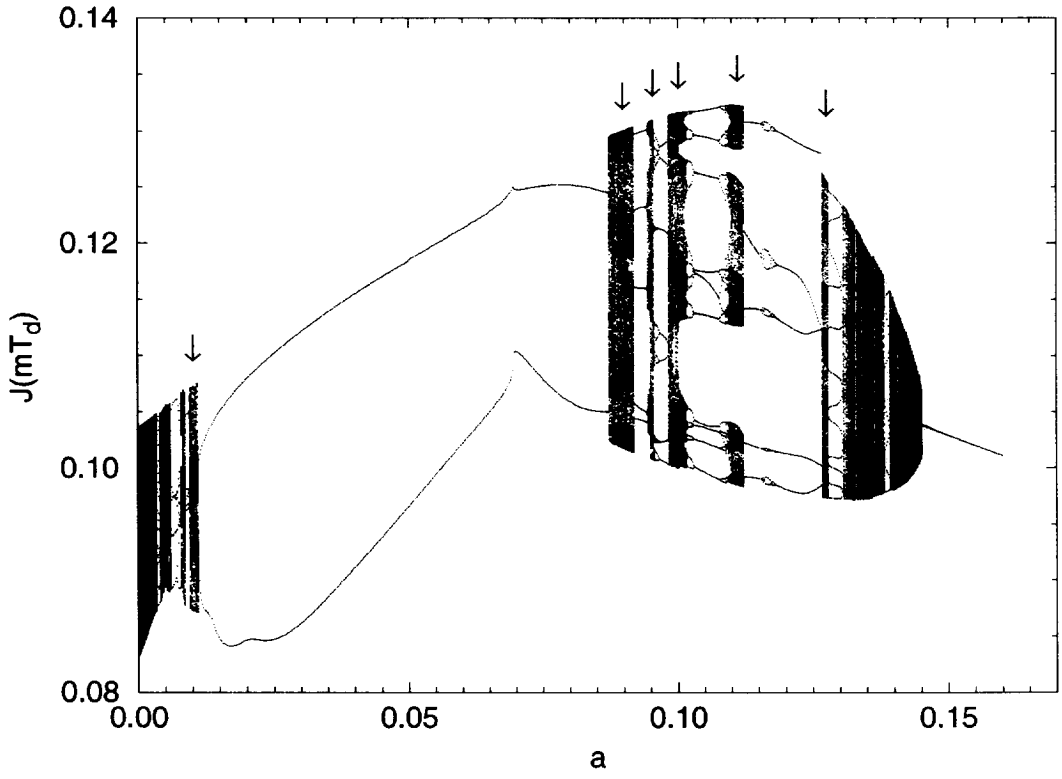

Fig. 4. Bifurcation diagram of the current at times mT_d (for sufficiently large m) vs the driving-force amplitude, for the golden-mean ratio between natural and driving frequencies. Windows of chaotic solutions are marked by arrows.

these monopoles is necessarily small. We have studied the influence of the number of SL wells on the spatial structure of chaotic solutions. For longer SLs ($N > 80$), we observe coexistence of up to three monopoles connecting four electric field domains during certain short time intervals; see Fig. 3c. Nucleation of monopole wavefronts occurs more frequently: in addition to long-living waves traveling over almost the whole SL, there are short-living waves. The two types of waves are distributed chaotically in space and nucleated both at the beginning and deep inside the SL. We have never observed more than three simultaneously present monopoles, even for unrealistically long SLs ($N = 500$). We speculate that the fast monopole nucleation is responsible for the loss of spatial coherence typical of the chaotic situation seen in Fig. 3c. If this is true, the fractal dimension of the chaotic attractor is related to the number of monopoles that can be simultaneously present on the SL: the more monopoles which coexist, the larger the dimension should be. Then we expect that the fractal dimensions of the chaotic attractors increase with SL length, and tend to saturate for SLs with more than 80 wells. This is confirmed by numerical simulations.

To detect and visualize the chaotic regions in parameter space, we adopt as Poincaré mapping (for each value of a) the current at times mT_d, $m = 0, 1, \ldots$ (after waiting enough time for the transients to have decayed)[10]. The result is the bifurcation diagram in Fig. 4. The chaotic regions marked by arrows are interspersed with locking to periodic regimes. To prove that statement we have computed the largest Lyapunov exponent and found it positive within chaotic windows and negative outside. Notice the period-doubling sequences that point to the existence of chaos near their accumulation points. Quasiperiodic routes to chaos have been found at the first and last windows, marked with arrows in Fig. 4, where the largest Lyapunov exponent was found to be zero. Notice that the period-2 orbits span the widest parameter region from the narrow chaotic band around $a \approx 0.01$ up to the next chaotic region at $a \approx 0.09$. For $a \geqslant 0.145$ the solution is attracted to the period-1 orbit with the driving frequency f_d.

In conclusion, our model describes in a satisfactory way, the stationary and dynamical properties of a weakly coupled semiconductor SL under a wide range of conditions. Low-dimensional chaos with loss of spatial coherence is expected to occur under appropriate d.c. + a.c. voltage bias for currently available n-doped GaAs/AlAs samples forming n^+-n-n^+ diodes[9].

Acknowledgements—We thank H. T. Grahn, J. Kastrup and R. Merlin for valuable discussions and collaboration. O. M. B. acknowledges the support of the Ministerio de Educación y Ciencia (Spain). This work was supported by the Spanish DGICYT grants PB92-0248 and PB94-0375.

REFERENCES

1. L. Esaki and L. L. Chang, *Phys. Rev. Lett.* **33,** 495 (1974).
2. K. K. Choi, B. F. Levine, R. J. Malik, J. Walker and C. G. Bethea, *Phys. Rev. B* **35,** 4172 (1987).
3. H. T. Grahn, R. J. Haug, W. Müller and K. Ploog, *Phys. Rev. Lett.* **67,** 1618 (1991).
4. S.-H. Kwok, Novel electric field effects in GaAs-(Al, Ga)As superlattices. Ph.D. thesis. University of Michigan, Ann Arbor. January, 1994. See also S.-H. Kwok, R. Merlin, L. L. Bonilla, J. Galán, J. A. Cuesta, F. C. Martínez, J. M. Molera, H. T. Grahn and K. Ploog, *Phys. Rev. B* **51,** 10171 (1995).
5. D. Miller and B. Laikhtman, *Phys. Rev. B* **50,** 18426 (1994).
6. L. L. Bonilla, J. Galán, J. A. Cuesta, F. C. Martínez and J. M. Molera, *Phys. Rev. B* **50,** 8644 (1994).
7. A. Wacker, F. Prengel and E. Schöll, *Phys. Rev. B* **50,** 1705 (1994).
8. L. L. Bonilla, in *Nonlinear Dynamics and Pattern Formation in Semiconductors and Devices* (Edited by F.-J. Niedernostheide), Chap. 1. Springer, Berlin (1995).
9. J. Kastrup, H. T. Grahn, K. Ploog and R. Merlin, Workbook of MSS-7, p. 254 (1995).
10. O. M. Bulashenko and L. L. Bonilla, *Phys. Rev. B* **52,** 7849 (1995).